

Improved WKB approximation for quantum tunneling: Application to heavy ion fusion

A. J. Toubiana^{1,2,3}, L. F. Canto^{4,5}, M. S. Hussein^{6,7,8}

¹ Departamento de Engenharia Nuclear, Escola Politécnica, Universidade Federal do Rio de Janeiro, C.P. 68529, 21941-909, Rio de Janeiro, RJ, Brazil,

² École CentraleSuplec, Plateau du Moulon 3, rue Joliot-Curie 91192 GIF-SUR-YVETTE - France,

³ Paris Saclay, Espace Technologique, Bat. Discovery - RD 128 - 2e t., 91190 Saint-Aubin, France,

⁴ Instituto de Física, Universidade Federal do Rio de Janeiro, CP 68528, Rio de Janeiro, Brazil,

⁵ Instituto de Física, Universidade Federal Fluminense, Av. Litoranea s/n, Gragoatá, Niterói, R.J., 24210-340, Brazil,

⁶ Instituto de Estudos Avançados, Universidade de São Paulo C. P. 72012, 05508-970 São Paulo-SP, Brazil, and Instituto de Física, Universidade de São Paulo, C. P. 66318, 05314-970 São Paulo,-SP, Brazil,

⁷ Departamento de Física Matemática, Instituto de Física, Universidade de São Paulo, C.P. 66318, 05314-970, São Paulo, SP, Brazil,

⁸ Departamento de Física, Instituto Tecnológico de Aeronáutica, CTA, São José dos Campos, São Paulo, SP, Brazil

December 27, 2022

Abstract. In this paper we revisit the one-dimensional tunnelling problem. We consider Kemble's approximation for the transmission coefficient. We show how this approximation can be extended to above-barrier energies by performing the analytical continuation of the radial coordinate to the complex plane. We investigate the validity of this approximation by comparing their predictions for the cross section and for the barrier distribution with the corresponding quantum mechanical results. We find that the extended Kemble's approximation reproduces the results of quantum mechanics with great accuracy.

PACS. 24.10Eq 25.70.Bc 25.60Gc

1 Introduction

Quantum tunneling (QT) has been with us for as long as the Schrödinger equation (SE). It describes a purely quantum phenomenon of a passage through a barrier. One of the first to popularize the essentials of QT was Gamow in his description of α decay of atomic nuclei. For this purpose, Gamow used an approximation of the solution of the SE based on the short wave length limit. This approximation came to be known as the WKB approximation and it corresponds to using the classical action as the phase of the wave function. In the development of the tunneling theory, several authors introduced concepts and recipes in order to get the tunneling probability as close as possible to the exact result obtained from the solution of the SE.

One such attempt was made by Kemble [1] who introduced a form for the probability which works at energies below the top of the barrier, attains the value 1/2 at the top of the barrier as the exact result dictates, but fails at energies above the barrier. Hill and Wheeler [2], used a parabolic form of the barrier which allows an exact analytical solution of the Schrödinger equation, which coincides with the result obtained using the Kemble formula for the same barrier for energies below the top of the barrier. The

HW form does work both below and above the barrier. However it has the major shortcoming that the parabolic approximation is only valid at energies in the vicinity of the top of the Coulomb barrier in nucleus-nucleus collisions.

In the current paper we discuss the approximation of the Coulomb barrier by a parabola, which is frequently adopted in the description of fusion of nuclei. In this case, the tunneling probability is called the transmission coefficient. The purpose of this paper is to demonstrate that the general WKB-based Kemble formula for the tunneling probability can be extended to the classically allowed region encountered at energies above the top of the barrier. With this extension we have a WKB formula for the tunneling probability valid for any well-behaved, complex nuclear potential at all energies. The paper is organized as follows. In section II, we discuss fusion reactions in heavy ions collisions. In Section III we discuss the WKB approximation as used in nuclear physics, and introduce the concept of fusion barrier distributions, which has attracted considerable interest over the last two decades. In section IV, we develop the extension of the Kemble formula to energies above the barrier top. This development is made for a typical potential for nucleus-nucleus colli-

sions. In section V, we use the approximations discussed in the previous section in the calculations of fusion cross sections and barrier distributions in the case of the light heavy ion system, ${}^6\text{Li} + {}^{12}\text{C}$. We chose a light system to stress the limitation of the parabolic approximation discussed in the present work. For heavy systems, this approximation works better. They do break down but this occurs at lower energies (in comparison to the Coulomb barrier). Finally, in Section VI several concluding remarks are presented.

2 Fusion reactions in heavy ion collisions

In a fusion reaction the projectile merges with the target, forming a compound nucleus (CN). The densities of the collision partners overlap so strongly that they lose their initial identities. Thus, the fraction of the incident current that reaches small projectile-target distances does not emerge in the elastic channel. In this way, any description of the collision based exclusively on the elastic channel violates the continuity equation. In multi-channel descriptions of the collision, this is not a problem because the current removed from the elastic channel re-emerges (after a time-delay) when the CN decays. However, if one adopts a single-channel approach, it is necessary to simulate the loss of flux in some way. This could be achieved through the introduction of a negative imaginary part in the projectile-target interaction potential, $W^F(r)$, or by adopting an ingoing wave boundary condition (IWBC).

In a heavy ion collision the real part of the potential has the general form,

$$V_l(r) = V_C(r) + V_N(r) + \frac{\hbar^2}{2\mu r^2} l(l+1), \quad (1)$$

where μ is the reduced mass of the projectile-target system, and V_C and V_N are respectively the Coulomb and the nuclear potentials. The third term in Eq. (1) is the centrifugal barrier, which appears in the radial equations. For the sake of definiteness, we consider the ${}^6\text{Li}-{}^{12}\text{C}$ collision throughout this paper.

As it is frequently done, we approximate the Coulomb potential as,

$$V_C(r) = \frac{Z_P Z_T e^2}{r}, \quad \text{for } r \geq R_C, \quad (2)$$

$$= \frac{Z_P Z_T e^2}{2R_C} \left(3 - \frac{r^2}{R_C^2} \right), \quad \text{for } r < R_C. \quad (3)$$

Above, Z_P and Z_T are respectively the atomic numbers of the projectile and the target, and e is the absolute value of the electronic charge. The *Coulomb radius*, R_C , is expressed in terms of the mass numbers of the projectile and the target (A_P and A_T) as $R_C = r_{0C} (A_P^{1/3} + A_T^{1/3})$, with $r_{0C} \simeq 1$ fm.

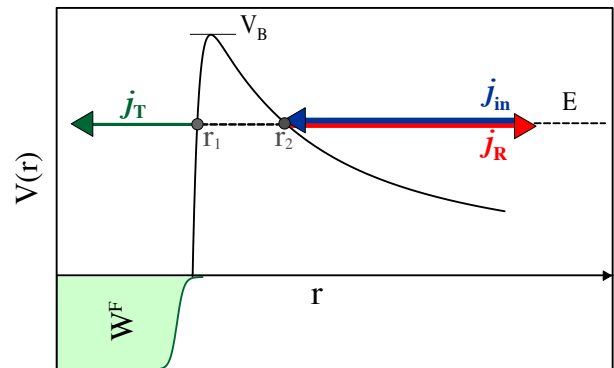


Fig. 1. (Color online) Schematic representation of the real and the imaginary potentials in a typical heavy ion collision. The classical turning points are indicated by r_1 and r_2 .

For $V_N(r)$, we adopt the Akyüz-Winther potential [3]. This potential is evaluated through a double folding integral of the nuclear densities with a M3Y [4] nucleon-nucleon interaction [5]. For practical purposes, it is approximated by the Woods-Saxon (WS) function

$$V_N(r) = \frac{V_0}{1 + \exp[(r - R_0)/a_0]}, \quad (4)$$

where $R_0 = r_0 (A_P^{1/3} + A_T^{1/3})$. The WS parameters of the Akyüz-Winther potential are expressed as functions of the mass numbers of the collision partners. For the ${}^6\text{Li}+{}^{12}\text{C}$ system they have the values: $V_0 = -31.35$ MeV, $r_0 = 1.16$ fm and $a_0 = 0.56$ fm.

In single-channel descriptions of fusion reactions based on Quantum Mechanics, one frequently uses a complex potential (the *optical potential*), whose real part is given by Eq. (1). The sum of the attractive nuclear potential with the repulsive Coulomb and centrifugal potentials gives rise to a potential barrier, with height V_B . The potential has also a negative imaginary part, W^F , very intense and with a short range, that accounts for the incident flux lost to the fusion channel. The situation is schematically represented in Fig. 1, for a collision energy (E) below the Coulomb barrier. The figure shows the incident current, j_{in} , the reflected current, j_R , and the current transmitted through the barrier, j_T , which reaches the strong absorption region. For practical purposes, the radial equation for each angular momentum is solved numerically. The numerical integration starts at $r = 0$, where the wave functions vanish and their derivatives are chosen arbitrarily. This choice only sets the normalization of the wave function, which has no influence on the cross sections.

Fusion absorption can also be simulated by an ingoing wave boundary condition (IWBC), with a real potential. In the IWBC [6,7,8] one makes the assumption that the radial wave function at some distance $r = R_{in}$ located in the inner region of the barrier (usually the minimum of $V_l(r)$) behaves as a wave propagating towards the origin. One then uses the WKB approximation to evaluate the

radial wave function and its derivative at $r = R_{\text{in}}$, and starts the numerical integration from this point.

The fusion cross section, can be evaluated by the partial-wave series

$$\sigma_F = \frac{\pi}{k^2} \sum_{l=0}^{\infty} (2l+1) P_l^F P_l^{\text{CN}} \quad (5)$$

where P_l^F is the absorption probability at the l^{th} partial-wave, given by

$$P_l^F = 1 - |S_l|^2, \quad (6)$$

and P_l^{CN} is the probability for the formation of the composite system, the compound nucleus, once the barrier is overcome. In most applications this probability is set equal to unity as the density of states of the CN is quite large. In light systems, such as $^{12}\text{C} + ^{12}\text{C}$, it was demonstrated by Jiang *et al.* [9] that at low energies the compound nucleus formation probability is significantly smaller than unity due to the low density of states of the CN, ^{24}Mg at the excitation energies involved. However, this phenomenon lies beyond the scope of the present paper. Thus, we will set $P_l^{\text{CN}} = 1$ for all values of the orbital angular momentum.

Owing to the imaginary potential, or to an IWBC, the S-matrix is not unitary. Instead, it satisfies the condition: $|S_l|^2 \leq 1$. The deviation from unitarity, $1 - |S_l|^2$, measures the absorption (fusion) probability. If absorption is simulated by the IWBC, there is no outgoing wave for $0 < r < R_{\text{in}}$. This means that the fraction of the incident current that reaches this region leads to fusion. Therefore, the fusion probability is given by the transmission coefficient through the potential barrier. Namely,

$$P_l^F \simeq T_l = \frac{j_{\text{T}}}{j_{\text{in}}}. \quad (7)$$

In principle, the IWBC is equivalent to the effects of a deep imaginary potential acting exclusively in the inner region of the barrier. One frequently assumes that the details of the imaginary potential do not have significant influence on fusion probabilities, as long as the potential is strong and has a short range. In fact, this assumption is questionable. It may be valid for heavier systems but it is not accurate in collisions of light heavy ions, like $^6\text{Li} - ^{12}\text{C}$. This fact is illustrated in Fig. 2, where the s-wave fusion probabilities obtained with the IWBC and with frequently adopted values of the radius parameter and the diffusivity are shown.

Besides studying the energy dependence of the fusion cross section, it was found useful to go further and study the quantity

$$\mathcal{D}_F(E) = \frac{d^2 [E\sigma_F(E)]}{dE^2}, \quad (8)$$

which is referred to as the *barrier distribution* [10,11]. Evaluating the second derivative numerically, experimental barrier distributions can be extracted directly from the

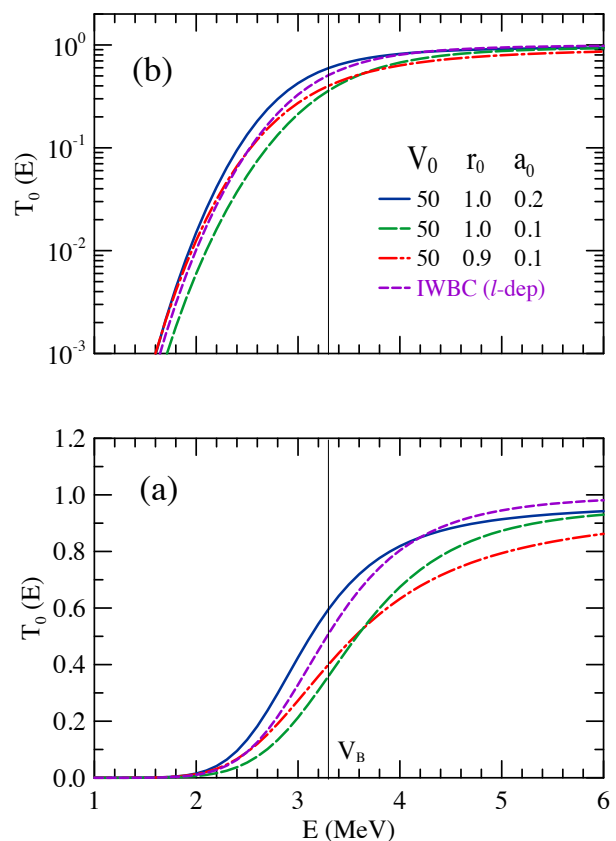


Fig. 2. (Color online) The transmission coefficient obtained with the IWBC and fusion probabilities evaluated with WS imaginary potentials with different r_0 and a_0 parameters (see the legend). The depth of the imaginary potential is kept fixed at $V_0 = 50$ MeV. The results are shown in linear (panel (a)) and logarithmic (panel (b)) scales.

data and comparing them with barrier distributions resulting from coupled channel calculations involving different channels, one can obtain invaluable information about the reaction mechanisms involved in the collision [12,13,14].

2.1 The Wong formula and barrier distribution

It has been a common practice in nuclear physics to use approximate forms of the potential barriers for the purpose of obtaining an analytical solution of the scattering Schrödinger equation using the IWBC, and thus getting an analytical form for the transmission coefficient. This has been first done by Hill and Wheeler [2], who approximated

$$V(r) = V_B - \frac{1}{2} \mu \omega (r - R_B)^2,$$

In the above equations, R_B is the barrier radius, V_B is the barrier height and $\hbar\omega$ is the curvature parameter,

$$\hbar\omega = \sqrt{\frac{-\hbar^2 V''(R_B)}{\mu}}.$$

The transmission coefficient through this barrier, known as the Hill-Wheller transmission coefficient, is given by the exact expression

$$T^{\text{HW}}(E) = \frac{1}{1 + \exp [2\Phi^{\text{HW}}(E)]},$$

with

$$\Phi^{\text{HW}}(E) = \frac{2\pi}{\hbar\omega} (V_{\text{B}} - E).$$

This approximation could be used for each partial wave, leading to angular momentum dependent barrier radii, heights and curvatures. In this way, one would have exact transmission coefficient for each l and, using them in the partial-wave expansion, one could obtain the fusion cross section.

Back in 1973, Wong [15] went one step further. He neglected the l -dependences of the barrier radii and curvatures, taking for all angular momenta the values for $l = 0$, denoted by R_{B} and $\hbar\omega$. In this way, the parabolic approximation for the effective potential is

$$V_l(r) = B_l - \frac{1}{2}\mu\omega (r - R_{\text{B}})^2, \quad (9)$$

where B_l is the barrier of the effective potential for the l^{th} partial-wave, given by

$$B_l = V_{\text{B}} + \frac{\hbar^2}{2\mu R_{\text{B}}^2} l(l+1). \quad (10)$$

He then treated the angular momentum quantum number as a continuous variable, $l \rightarrow \lambda = l + 1/2$, and approximated the sum of partial-waves by an integral over λ . In this way, he got the closed expression,

$$\sigma_{\text{F}}^{\text{W}}(E) = \frac{\hbar\omega R_{\text{B}}^2}{2E} \ln \left[1 + \exp \left(\frac{2\pi}{\hbar\omega} (E - V_{\text{B}}) \right) \right]. \quad (11)$$

Eq. (11), known as the Wong formula, has been quite popular in low energy heavy-ion fusion and reactions.

The fusion barrier distribution associated with the Wong formula can be evaluated easily. Using the cross section of Eq. (11) in Eq. (8), one gets

$$\mathcal{D}_{\text{F}}^{\text{W}}(E) = \frac{\pi^2 R_{\text{B}}^2 / \hbar\omega}{1 + \cosh [2\pi (E - V_{\text{B}}) / \hbar\omega]}. \quad (12)$$

3 The WKB approximation in Nuclear Physics

The WKB approximation is a short wavelength limit of Quantum Mechanics. Since it is extensively discussed in text books on Quantum Mechanics and Scattering Theory [16,17,5], its derivation will not be presented here. We consider only some applications in scattering theory. We discuss the WKB approximation in the calculation of the transmission coefficients used to determine fusion

cross sections (Eqs. (5) and (7)).

Let us consider the ${}^6\text{Li} - {}^{12}\text{C}$ collision at a sub-barrier energy E , as represented in Fig. 1. Within the WKB approximation, the transmission coefficient through the barrier of the l^{th} partial-wave is given by

$$T_l^{\text{WKB}}(E) = \exp [-2\Phi_l^{\text{WKB}}(E)]. \quad (13)$$

Above, Φ_l^{WKB} is the integral

$$\Phi_l^{\text{WKB}}(E) = \int_{r_1}^{r_2} \kappa_l(r) dr, \quad (14)$$

where

$$\kappa_l(r) = \frac{\sqrt{2\mu [V_l(r) - E]}}{\hbar}. \quad (15)$$

In the above equations, r_1 and r_2 are the classical turning points, indicated in Fig. 1. They are the solutions of the equation on r ,

$$V_l(r) = E. \quad (16)$$

Eq. (13) works very well for collision energies well below the Coulomb barrier, but it becomes very poor near the Coulomb barrier and above. At $E = B_l$, the two classical turning points coalesce, so that $\Phi_l^{\text{WKB}}(E) = 0$. In this way, one gets $T_l^{\text{WKB}}(E) = 1$, whereas the quantum mechanical result is $T_l^{\text{QM}}(E) = 1/2$.

In 1935, Kemble [1] showed that the WKB approximation can be improved if one uses a better connection formula. He got the expression

$$T_l^{\text{K}}(E) = \frac{1}{1 + \exp [2\Phi_l^{\text{WKB}}(E)]}. \quad (17)$$

At energies well below the Coulomb barrier, the two turning points are far apart and $\kappa(r)$ reaches appreciable values within the integration limits. In this way, $\Phi^{\text{WKB}}(E)$ becomes very large, so that the unity can be neglected in the denominator of Eq. (17). This equation then reduces to Eq. (13). Therefore, the two approximations are equivalent in this energy region. On the other hand, Kemble's approximation remains valid as the energy approaches the Coulomb barrier, so that at $E = B_l$ one gets $\Phi^{\text{WKB}}(E) = 1/2$, which is the correct result.

Unfortunately, Eq. (17) gives wrong results at above-barrier energies. In this energy range, there are no classical turning points, since Eq. (16) has no real solutions. Thus, $\Phi^{\text{WKB}}(E) = 0$. In this way, the transmission coefficient is frozen at the value $1/2$. Therefore, it has the wrong high energy limit. However, Kemble [1] pointed out that the validity of Eq. (17) could be extended to above-barrier energies by an analytical continuation of the variable r to the complex plane (see also Ref. [18]), although he did not elaborate on it. This point is considered in detail in the next section.

4 Kemble transmission coefficient at above-barrier energies

Eq. (17) can be extended to above-barrier energies if one solves Eq. (16) in the complex r -plane and evaluates the integral of Eqs. (14) and (15) between the complex turning points. In this section, we apply this procedure to a typical potential in heavy ion scattering, and show that it actually works.

First, we introduce the dimensionless coordinate

$$r \rightarrow x = \frac{r - R_B}{a_0}, \quad (18)$$

where R_B is the barrier radius and a_0 is the diffusivity parameter of the WS potential. Next, this coordinate is extended to the complex plane. That is: $x \rightarrow z = x + iy$. The effective potential of Eq. (1) then becomes,

$$V_l(z) = \frac{V_0}{1 + \exp(z + d)} + \frac{Z_P Z_T e^2}{a_0 z + R_B} + \frac{\hbar^2 (l + 1/2)^2}{2\mu (a_0 z + R_B)^2}. \quad (19)$$

Above,

$$d = \frac{R_B - R_0}{a_0}$$

is a dimensionless constant, associated with the difference between the barrier radius and the radius of the nuclear potential. Note that in Eq. (19) we replaced $l(l + 1) \rightarrow (l + 1/2)^2$. This is a common procedure in semiclassical theories.

Then, writing the now complex effective potential as,

$$V_l(z) \equiv V_l(x + iy) = U_l(x, y) + iW_l(x, y),$$

one imposes that its imaginary part vanishes. That is,

$$W_l(x, y) \equiv \text{Im}\{V_l(z)\} = 0. \quad (20)$$

We should remind that the complexity of the potential is of purely mathematical origin and should not be confused with absorption of flux. Using the explicit form of the effective potential (Eqs. (1), (2) and (4)) in Eq. (20), one gets a complicated equation, that describes lines on the complex z -plane.

Solving Eq. (20) by a numerical procedure, one gets the curve Γ represented by a blue dashed line on panel (a) of Fig. 3. We remark that there are other curves on the complex plane where the potential is real. First, there is a curve Γ' , at the left of Γ . That is, for $x < -d$. It looks like a distorted reflection of Γ around a vertical axis at $x = -d$. In this way, joining this curve with Γ , one gets a closed contour. The potential is also real on other curves with $|y| > \pi$. The shapes of these curves are expected to be different from Γ , because the Coulomb and

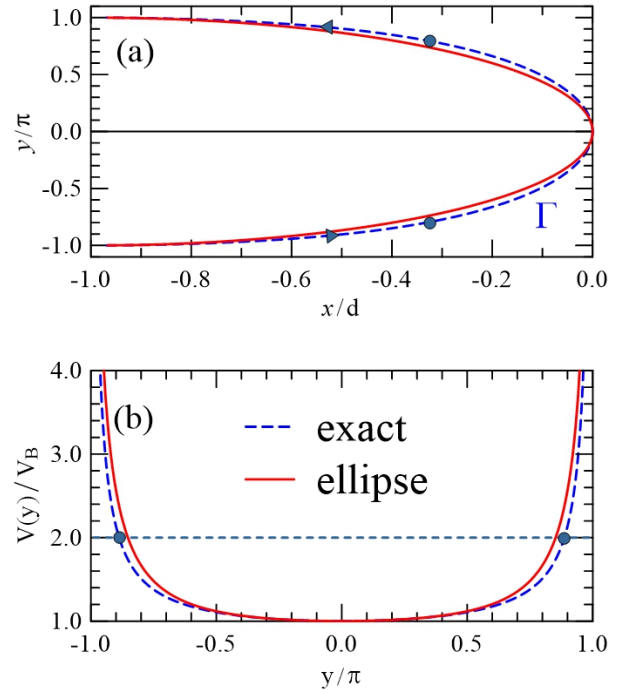


Fig. 3. (Color online) The analytic continuation of the real potential of Eq. (1). Panel (a) shows the curves Γ (blue dashed line) and Γ_e (red solid line), and panel (b) shows the corresponding real potentials on these lines. For details, see the text.

the centrifugal potentials are not periodic in y . However, the physics involved in the collision is fully described by the analytical continuation on Γ . Therefore, we restrict our discussion to this curve.

We find that the curve Γ is very close to the ellipse Γ_e given by the equation,

$$\left(\frac{x + d}{d}\right)^2 + \left(\frac{y}{\pi}\right)^2 = 1. \quad (21)$$

This ellipse is represented in Fig. (3) by a red solid line. Clearly, the elliptical approximation for Γ is indeed quite good.

Now we consider the potential over the contour Γ . Owing to Eq. (20), we can express x as a function of y , $x_\Gamma(y)$, so that the corresponding complex coordinate becomes,

$$z_\Gamma(y) = x_\Gamma(y) + iy. \quad (22)$$

In this way, the potential depends exclusively on the coordinate y . To simplify the notation of the potential over Γ , where it is real, we write

$$U_\Gamma(y) = V_l(z_\Gamma(y)). \quad (23)$$

Since Eq. (20) is rather complicated, the function $x_\Gamma(y)$ cannot be obtained analytically. Therefore, the potential $U_\Gamma(y)$ must be determined numerically.

The situation is much simpler within the elliptical approximation for Γ . Using Eq. (21), we get

$$x_{\Gamma_e}(y) = -d \left[1 - \sqrt{1 - \frac{y^2}{\pi^2}} \right].$$

Inserting the above equation into Eq. (22), and using the result in Eq. (19), we get an analytical expression for the potential $V_l(z_{\Gamma_e}(y))$. However, this potential is not exactly real. Owing to the approximation of Γ by Γ_e , $V_l(z_{\Gamma_e}(y))$ has a small imaginary part, which should be discarded. We then write,

$$U_{\Gamma_e}(y) = \text{Re} \left\{ V_l(z_{\Gamma_e}(y)) \right\}. \quad (24)$$

This potential, evaluated for $l = 0$, corresponds to the red solid line in Fig. (3) (b). Clearly it is very close to the exact potential.

Inspecting $U_{\Gamma}(y)$, one immediately notices that it goes to infinity at the two extremes of the plot, which correspond to $y = \pm\pi$. These divergences can be traced back to the poles of the WS potential, located at $r = R_0 + in\pi$, where n is any positive or negative integer. In terms of z , the poles are located at $z = -d + in\pi$. The infinite value of the potential at $y = \pm\pi$ has two important consequences. The first is that it confines the complex plane to the region $-\pi < y < \pi$, which corresponds to $-d < x < 0$. In this way, the curve Γ' and curves with $|y| > \pi$ are not accessible to the system. Thus, such curves can be completely ignored. The second consequence is that the minimal value of x on Γ is $x = -d$, which corresponds to $r_{\min} = R_0$ and this value is larger than R_c . Therefore, the Coulomb potential for points on Γ are always given by Eq. (2). This justifies our choice of the Coulomb potential in Eq. (19).

From Fig. 3 we conclude that ellipse is very close to Γ , and the potentials over the two curves are nearly the same. Thus, we henceforth replace the contour Γ by the approximate curve Γ_e . This simplifies our calculations considerably.

Now we evaluate Kemble's transmission factor. For this purpose, one has to calculate the WKB integral between the complex turning points, z_{\pm} ,

$$\Phi^{\text{WKB}}(E) = a_0 \frac{\sqrt{2\mu}}{\hbar} \int_{z_-}^{z_+} dz \sqrt{V_l(z_{\Gamma_e}) - E}. \quad (25)$$

We remark that the factor a_0 results from the change of variable of Eq. (18). The integral of Eq. (25) is independent of the integration path on the complex-plane. It depends only on the integration limits, z_- and z_+ . However, for practical purposes, it is convenient to evaluate the integral along the contour Γ_e . On this contour, $V_l(x, y)$ reduces to the real potential of Eq. (24), $U_{\Gamma_e}(y)$, and the differential dz can be written as

$$dz = \left[\frac{dx_{\Gamma_e}(y)}{dy} + i \right] dy,$$

where $dx_{\Gamma_e}(y)/dy$ is a real function of y . For energies above the barrier, $U_{\Gamma_e}(y) - E$ is negative so that,

$$\begin{aligned} dz \sqrt{U_{\Gamma_e}(y) - E} &= \left(\frac{dx_{\Gamma_e}(y)}{dy} + i \right) \times i \sqrt{E - U_{\Gamma_e}(y)} dy \\ &= G_R(y) dy + i G_I(y) dy, \end{aligned} \quad (26)$$

where $G_R(y)$ and $G_I(y)$ are the real functions,

$$G_R(y) = -\sqrt{E - U_{\Gamma_e}(y)}, \quad (27)$$

$$G_I(y) = \frac{dx_{\Gamma_e}(y)}{dy} \sqrt{E - U_{\Gamma_e}(y)}. \quad (28)$$

The values of y corresponding to the integration limits of Eq. (25) are given by the equation,

$$U_{\Gamma_e}(y) = E.$$

They are schematically represented in Fig. (3), for the collision energy $E = 2V_B$. Since the potential $U_{\Gamma_e}(y)$ is symmetric with respect to $y = 0$, the turning points have the property,

$$y_- = -y_+. \quad (29)$$

Thus, Eq. (29) indicates that the integration limits are symmetric. This property can be formally proved. Since $F(z) \equiv E - V_l(z)$ is an analytic function of z in the vicinity of Γ (or Γ_e), we can write $F^*(z) = F(z^*)$. Thus, if z_+ is a complex turning point, that is, it satisfies the equation $F(z_+) = 0$, $z_- = z_+^*$ will also be a turning point. Then, writing $z_+ = x_+ + iy_+$, the other turning point, will be $z_- = x_- + iy_-$, with $x_- = x_+$ and $y_- = -y_+$.

Expressing the integral of Eq. (25) in terms of the variable y , one gets

$$\begin{aligned} \Phi^{\text{WKB}}(E) &= a_0 \frac{\sqrt{2\mu}}{\hbar} \text{Re} \left\{ \int_{y_-}^{y_+} G_R(y) dy \right. \\ &\quad \left. + i \int_{y_-}^{y_+} G_I(y) dy \right\}. \end{aligned} \quad (30)$$

Fig. 3(a) indicates that the potential $U_{\Gamma_e}(y)$ is an even function of y , and so is the function $G_R(y)$ of Eq. (27). On the other hand, inspecting Fig. 3(b) one concludes that $dx_{\Gamma_e}(y)/dy$ is an odd function of y . For this reason, the function $G_I(y)$ of Eq. (28) is odd. Since the integration limits in Eq. (30) are symmetric, the second integral in this equation vanishes. Then, the WKB integral reduces to,

$$\Phi^{\text{WKB}}(E) = -a_0 \frac{\sqrt{2\mu V_B}}{\hbar} \int_{y_-}^{y_+} dy \sqrt{\varepsilon - \frac{U_{\Gamma_e}(y)}{V_B}}.$$

Above, we have introduced the notation,

$$\varepsilon = \frac{E}{V_B}.$$

Inserting Eq. (4) into (Eq. (17)), one gets Kemble's transmission coefficient at above-barrier energies.

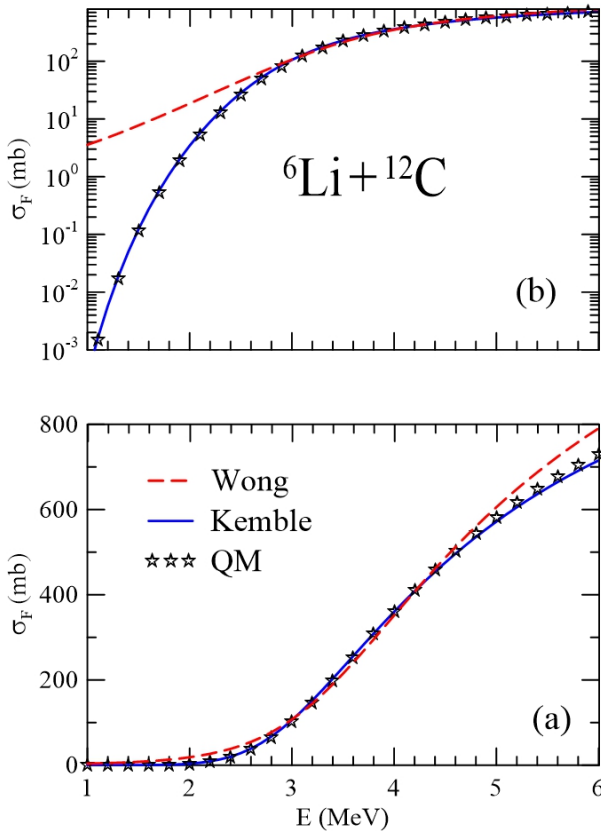


Fig. 4. (Color online) Comparison of the exact quantum mechanical fusion cross section for the ${}^6\text{Li} + {}^{12}\text{C}$ systems with results of approximations discussed in the previous sections. The results are shown in linear (panel (a)) and logarithmic (panel (b)) scales.

5 Study of fusion in the ${}^6\text{Li} - {}^{12}\text{C}$ collision

Now we discuss the use of the approximations of the previous sections to predict observable quantities. First we look at fusion cross sections. We compare the exact cross section, obtained with full quantum mechanics, with the cross section obtained with Kemble's WKB transmission coefficients through the exact barriers. In all Kemble-WKB calculations, we used the elliptical approximation for Γ . We consider also the Wong cross section, which is evaluated with exact transmission coefficients but through approximate l -dependent barriers. The results are shown in Fig. 4, in linear (panel (a)) and logarithmic (panel (b)) scales. The cross sections obtained with the Wong formula, with Kemble's WKB and with full quantum mechanics are respectively represented by the red dashed line, the blue solid line and by stars.

One finds that Wong's approximation is good at near-barrier energies, but it becomes progressively worse as the energy decreases. At the lowest energies in the plot, $E \sim 1$ MeV, it overestimates the quantum mechanical cross section by more than three orders of magnitude. One notices also that Wong's approximation gets worse at energies above ~ 4.5 MeV. The reason is that, as the energy

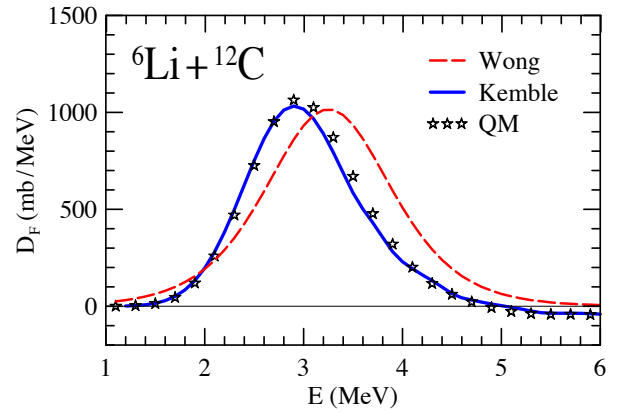


Fig. 5. (Color online) Barrier distributions for the fusion cross sections of the previous figure.

increases, Wong's cross section gets relevant contributions from higher partial-waves, where the radius and the curvature parameters become significantly different from those for $l = 0$. These differences are ignored in the derivation of the formula. The situation with Kemble's approximation is completely different. The stars, which represent the quantum mechanical calculation, falls on top of the blue solid line, corresponding to Kemble's WKB.

Now we discuss the predictions of the same calculations for the fusion barrier distributions. The results are presented in Fig. 5. The notation is the same as in the previous figure. Since barrier distributions are always calculated near the barrier, Wong's barrier distribution is not too bad. It is in qualitative agreement with the quantum mechanical fusion barrier distribution. On the other hand, the results of Kemble's WKB are extremely good. They reproduce the exact barrier distribution throughout the energy region of the figure. An interesting aspect of the figure is that the maximum of the quantum mechanical barrier, and also of Kemble's barrier distribution, occurs at $E_{\text{max}} = 2.95$ MeV. Although is not far from the barrier of the bare potential ($V_B = 3.25$ MeV), it is about 0.3 MeV lower.

6 Conclusions

In this paper we considered the more general, and potentially more useful, Kemble approximation for the tunnelling probability, which is an improved version of the WKB approximation. We considered in detail the extension of Kemble's approximation to energies above the barrier, which can be achieved by judicious contour integration in the complex r -plane. By a judicious choice of a contour in the complex r -plane we have extended the validity of the Kemble formula to energies above the barrier. We have accomplished this for barriers of a typical optical potential in heavy ion collisions.

We have discussed also cross sections and barrier distributions, as given by the second derivative of $E\sigma_F$ with

respect to energy, and shown that Kemble's approximation gives an exceedingly good description of the quantum mechanical results at near-barrier energies. Thus we have, in this paper, finally obtained a WKB tunneling probability which is valid for an arbitrary potential and at all energies, without relying on the parabolic or other approximation.

We are grateful to Kouichi Hagino for providing us with a single-channel code using the ingoing wave boundary condition, and to Raul Donangelo for critically reading the manuscript. Partial support from the Brazilian funding agencies, CNPq, FAPESP, and FAPERJ is also acknowledged. M. S. H. acknowledges support from the CAPES/ITA Senior Visiting Professor Fellowship Program A.J.T. acknowledges financial support from the French committee of the Brafitec program.

References

1. E.C. Kemble, Phys. Rev. **48**, 549 (1935)
2. D.L. Hill, J.A. Wheeler, Phys. Rev. **89**, 1102 (1953)
3. R.A. Broglia, A. Winther, *Heavy Ion Reactions* (Westview Press, 2004)
4. G.F. Bertsch, J. Borysowicz, H. McManus, W.G. Love, Nucl. Phys. **A284**, 399 (1977)
5. L.F. Canto, M.S. Hussein, *Scattering Theory of Molecules, Atoms and Nuclei* (World Scientific Publishing Co. Pte. Ltd., 2013)
6. G.H. Rawitscher, Phys. Rev. **135**, B605 (1964)
7. G.H. Rawitscher, Nucl. Phys. **85**, 337 (1966)
8. K. Hagino, N. Rowley, A.T. Kruppa, Comp. Phys. Commun. **123**, 143 (1999)
9. C.L. Jiang, B.B. Back, H. Esbensen, R.V.F. Janssens, K.E. Rehm, R.J. Charity, Phys. Rev. Lett. **110**, 072701 (2013)
10. N. Rowley, G.R. Satchler, P.H. Stelson, Phys. Lett. B **254**, 25 (1991)
11. K. Hagino, N. Rowley, Phys. Rev. **C69**, 054610 (2004)
12. M. Dasgupta, D. Hinde, N. Rowley, A. Stefanini, Ann. Rev. of Nucl. Part. Sci. **48**, 401 (1998)
13. L.F. Canto, , P.R.S. Gomes, R. Donangelo, M.S. Hussein, Phys. Rep. **424**, 1 (2006)
14. L.F. Canto, P.R.S. Gomes, R. Donangelo, J. Lubian, M.S. Hussein, Phys. Rep. **596**, 1 (2015)
15. C.Y. Wong, Phys. Rev. Lett. **31**, 766 (1973)
16. E. Merzbacher, *Quantum Mechanics*, 3rd edn. (John Wiley & Sons, Inc., 1998)
17. C.J. Joachain, *Quantum Collision Theory* (North Holland, 1983)
18. N. Fröman, P. Fröman, *JWKB Approximation: Contributions to the Theory*, 1st edn. (North-Holland, Amsterdam, 1965)